OPEN ACCESS

UNIVERSITY OF DUNDEE

University of Dundee

Root branching affects the mobilisation of root-reinforcement in direct shear

Meijer, Gerrit J.; Wood, David Muir; Knappett, Jonathan A.; Glyn Bengough, A.; Liang, Teng

Root branching affects the mobilisation of root-reinforcement in direct shear

Gerrit J. Meijer[1,*], *David* Muir Wood[1], *Jonathan A.* Knappett[1], *A. Glyn* Bengough[1,2], and *Teng* Liang[1]

[1]University of Dundee, School of Science and Engineering, Dundee DD1 4HN, UK
[2]The James Hutton Institute, Invergowrie, Dundee DD2 5DA, UK

Abstract. The contribution of roots to the mechanical behaviour of soil has typically only been studied for the ultimate limit state. In these approaches, roots are typically modelled as straight and unbranched structures. This approach overlooks the fact that roots may have to deform significantly to mobilise their strength, a process that will be influenced by root architecture effects such as branching, amongst others. Sequential mobilisation of roots affects the peak root-reinforcement, thus differences in mobilisation are important to consider when quantifying root-reinforcement. In this paper, the effect of root branching was modelled using a large-deformation Euler-Bernoulli beam-spring model. The effect of soil was incorporated using non-linear springs, similar to *p-y* and *t-z* theory used for foundation piles. By connecting multiple beams together (i.e. applying appropriate linked boundary conditions at root connection points) the effect of branching could be analysed. A soil displacement profile corresponding with direct shear loading was then imposed and the response of the root analysed. It was shown that adding branches led to a quicker mobilisation of root-reinforcement. Branches increased the axial resistance to root displacement and changed the shape of the deformed roots. The presence of branching counteracted root slippage, and thus increased reinforcement. Larger branching densities increased this effect. This analysis demonstrated that the architecture of the root system has a strong effect on the mobilisation of root strength, which directly affects the maximum amount of reinforcement the roots will provide. Future modelling of root-reinforcement, both at the ultimate and serviceable limit state, should account for this effect.

1 Introduction

The reinforcement of soil by roots can be split into a hydrological component (change of matric suction due to plant evapotranspiration) and a mechanical component (reinforcement through mechanical action of root). In this paper, the focus is on mechanical reinforcement. Typically, root-reinforcement is studied in the context of slope stability [1], resulting in a focus on the ultimate limit strength of the rooted soil. In this case, the contribution of roots is often incorporated into models as an increase in soil cohesion [2]. Often, the critical slope stability case will be when the ground is fully saturated, meaning hydrological reinforcement disappears.

This focus on the ultimate limit state overlooks that significant deformations might be required to mobilise root strength. For structures with tight deformation tolerances however, for example rooted railway embankments or cuttings, these deformations might exceed the serviceability limit state. To investigate the contribution of roots in such cases, greater insight is required in the mobilisation behaviour of rooted soil.

However, even when only the ultimate limit state is of interest, mobilisation of root strength is important to consider. The natural variation in root properties such as root

diameter, root stiffness root angle or root branching will lead to sequential mobilisation of the strength of individual roots; some roots will mobilise their strength faster, for example due to preferential orientations or large root stiffness, and might have broken already by the time other roots mobilise. In practice, the contribution of this effect on the ultimate limit state of the soil is often taken into account through the use of a root cohesion reduction factor based on fibre bundle theory [3]. Such an approach, although pragmatic, does not provide any insight into the underlying physical mechanisms, thus being of limited use for systematic study of root–soil interaction.

One promising approach to increase understanding of root–soil interaction is to model roots as mechanical beams. Euler-Bernoulli beam theory has been adopted previously to model thick, individual roots by various authors [4, 5]. Recently, this concept was developed further by coupling axial and bending behaviour and taking into account large root deformations [6], thus making this approach suitable for both thick and thin roots for realistic slope deformations.

Currently, models for root-reinforcement are often based on the assumption that roots are straight, unbranched cylindrical structures. Beam theory however allows for modelling more realistic root architectures by modelling root systems as sets of connected beams. Such

---
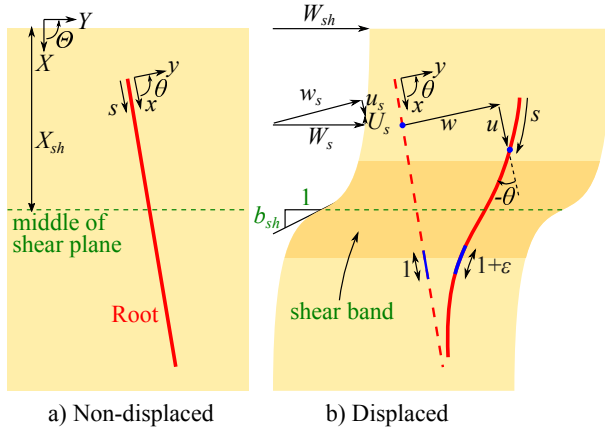
*e-mail: g.j.z.meijer@dundee.ac.uk

Fig. 1. Coordinate systems and definitions (see text section 2.1 for details)

an approach was used in this paper to study the effect of root branching on the mobilisation of root strength in direct shear tests.

2 Methodology

2.1 Model description

Roots systems are modelled as individually connected two-dimensional beam segments. Each segment has a local coordinate system (x,y), where the x axis is aligned with the non-displaced root segment axis. Positions and deformations in the global coordinate system (X,Y) are indicated using capitals. X indicates depth, with $X = 0$ corresponding to the soil surface level, see Figure 1a.

Root segments are modelled as linear elastic, spring supported beams following Euler-Bernoulli beam theory. Roots are flexible compared to structural piles with Young's moduli of around 100 MPa [7] and tensile strains to failure of around 15–20% [8]. Therefore, conventional beam theory needs to be extended to account for large deformations. To accommodate this, the root behaviour is described in a coordinate system aligned with the axis of the deformed root s, see Figure 1b.

The methodology as set out by [6] was followed, describing the behaviour of the root using four coupled differential equations. The first equation accounts for axial deformations along the deformed root axis s:

$$- q_a = \frac{\partial N}{\partial s} + \frac{\partial M}{\partial s}\frac{\partial \theta}{\partial s} \qquad (1)$$

where M and N are the internal root bending moment and normal force, q_a is the external axial load due to root–soil interface friction along the root axis (force per unit of non-displaced root length), θ the root deflection angle between axes x and s, and ϵ the axial root strain.

A second differential equation describes the behaviour in bending:

$$\frac{\partial^2 M}{\partial s^2} = q_l + N\frac{\partial \theta}{\partial s} \qquad (2)$$

where q_l is the transverse root–soil interaction load. It is assumed that the root axial strain does not affect the internal root bending moment M through a change in root length (theoretically, when the root becomes longer, bending moments might increase slightly due to an increase in the length of the lever arm).

The axial force N follows directly from the axial stain in the root:

$$N = E_t A \epsilon \qquad (3)$$

where E_t is the root tensile stiffness and A the root cross-sectional area. The bending moment M is equal to the product of the root flexural rigidity and root curvature. It is assumed that the root axial strains are sufficiently small so that the effect of ϵ on the root curvature can be ignored. Therefore:

$$M = E_b I \frac{\partial \theta}{\partial s} \qquad (4)$$

where E_b is the root bending stiffness and I the second moment of area of the root cross-section.

The final two differential equations link the deformations u and w in the local root segment coordinate system (x,y) to the deformations (θ,ϵ) in the coordinate system local the the root (s):

$$\frac{\partial u}{\partial s} = (1 + \epsilon)\cos\theta - 1 \qquad (5)$$

$$\frac{\partial w}{\partial s} = (1 + \epsilon)\sin\theta \qquad (6)$$

The magnitude of axial and transverse resistances q_a and q_l depends on the relative soil–root displacement. Simplifying from [6], these relative deformations are taken as the relative displacements in the undeformed local root segment coordinate system:

$$q_a = q_{a,u} \tanh\left(\frac{u_s - u}{b_a}\right) \qquad (7)$$

$$q_l = q_{l,u} \tanh\left(\frac{w_s - u}{b_l}\right) \qquad (8)$$

where $q_{a,u}$ and $q_{l,u}$ are the ultimate axial and transverse soil resistances that can be mobilised, b_a and b_l mobilisation parameters, and u_s and w_s the axial and transverse soil deformations in the local root segment coordinate system (x,y), see Figure 1. Direct shear box tests are modelled using the following profile of soil deformations U_s (in global X-direction) and W_s (in global Y-direction):

$$U_s = 0 \qquad (9)$$

$$W_s = W_{sh}\left[\frac{1}{2} - \frac{1}{2}\tanh\left(\frac{X - X_{sh}}{b_{sh}}\right)\right] \qquad (10)$$

where W_{sh} is direct shear displacement in the Y-direction, X_{sh} the depth of the middle of the shear band and b_{sh} a shear band shape parameter. All of these are input parameters in the model. The soil deformations u_s and w_s in the local root coordinate system x,y are simply found from U_s and W_s using coordinate transformation.

The maximum axial soil–root resistance is modelled as the sum of adhesive and frictional components:

$$q_a = \pi d_r (a_i + \sigma'_n \tan \delta) \tag{11}$$

where d_r is the root diameter, σ'_n the root confining stress, δ_i the root–soil interface friction angle and a_i the interface adhesion. For simplicity, the maximum transverse soil–root resistance is modelled using bearing capacity factors N_q and N_c:

$$q_l = d_r \left(N_c c' + N_q \sigma'_n \right) \tag{12}$$

where c' is the soil cohesion.

When the modelled root systems consists of multiple connected root segments, Equations 1, 2, 5 and 6 are simultaneously solved for all segments, taking into account appropriate boundary conditions where segments connect, see [6].

Thus, when soil strength properties, interface properties, root properties and the soil deformation profile are known or assumed, the deformation and internal forces in the entire root system architecture can be modelled by solving all differential equations simultaneously. This was done using a boundary value problem solver in Python (`solve_bvp` function from the `integrate` package within the `scipy` library [9]).

The root-reinforcement F_r then follows from decomposition of internal root forces in the middle of the shear band into a component parallel ($F_{r,par}$) and perpendicular to the shear direction ($F_{r,per}$):

$$F_r = F_{r,par} + F_{r,per} \tan \phi' \tag{13}$$

where ϕ' is the soil angle of internal friction. The latter terms accounts for reinforcement through an increase in confining stress in the shear band.

The axial stress (σ_a) and bending strengths (σ_b) in the root are defined as:

$$\sigma_a = \frac{N}{A} = E_t \epsilon \tag{14}$$

$$\sigma_b = \frac{Md}{2I} = \frac{E_b d_r}{2} \frac{\partial \theta}{\partial s} \tag{15}$$

where d is the root diameter.

2.2 Direct shear testing

Direct shear tests performed on rooted soil samples in an X-Ray Computed Tomography (CT) scanner by [10] are used to develop realistic modelling scenarios. In these tests, 500 mm tall, 100 mm diameter tubes were filled with Bullionfield soil [7, 10, 11], planted with willow (*Salix viminalis* Tora) cuttings that were then grown for two months. Cores were subsequently saturated, drained and sheared at 250 mm depth while maintaining a water potential of $\psi = 0$ kPa at the base of the core (so $\psi = -5$ kPa at the top of the core). Samples were sheared at 1 mm min^{-1} to a maximum displacement of 20 mm. The corresponding stress conditions were modelled assuming:

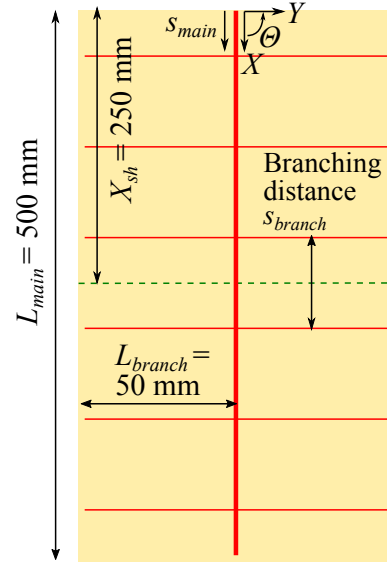$$\sigma' = \gamma X - \chi \psi \tag{16}$$

Fig. 2. Branching scenario modelled

For simplicity, $\chi = 1$, soil unit weight $\gamma = 10$ kNm^{-3} and a coefficient of lateral earth pressure $K_0 = 1$ were assumed. In this case, the increase in effective stress with depth due to the self weight of the soil was cancelled out by the reduction in suction pressure, resulting in a constant, isotropic effective stress of $\sigma' = 5$ kPa (and $\sigma'_n = \sigma'$) throughout the entire core.

The largest roots observed in the CT data had diameters of $d_{main} \approx 1.5$ mm and were assumed to grow vertically to the very bottom of the core ('main' root axis, root length $L_{main} = 500$ mm). First-order branches had diameters of roughly $d_{branch} \approx 0.5$ mm. The length of these branches was assumed as half the core diameter, $L_{branch} = 50$ mm. The tensile root strength and tensile stiffness of willow roots this age are $t_r \approx 11$ MPa and $E_t \approx 200$ MPa respectively [7]. For simplicity, the bending stiffness E_b was assumed equal to the tensile stiffness E_t.

The shear band thickness was approximately 30 mm thick (CT observations), resulting in $b_{sh} \approx 10.2$ mm. The soil is assumed purely frictional with $\phi' = 36.4°$ [7] and $c' = 0$ kPa respectively. Following Meyerhoff bearing capacity theory:

$$N_q = e^{\pi \tan \phi'} \tan^2 \left(\frac{\pi}{4} + \frac{\phi'}{2} \right) \approx 40 \tag{17}$$

$$N_c = (N_q - 1) \cot \phi' \approx 53 \tag{18}$$

The axial root–soil interface friction is modelled as purely frictional and perfectly rough, so the interface friction angle $\delta_i = \phi'$ and adhesion $a_i = 0$. No data for soil–root resistance mobilisation was available, hence $b_a = 0.5$ mm and $b_l = 0.1$ mm were assumed, similar to values in [6].

2.3 Modelling scenarios

The following scenarios were modelled (Figure 2):

1. Modelling of roots in the CT scan, see section 2.2. Multiple pairs of side branches were modelled at either side of the shear band. The effect of the distances between branches (branching distance s_{branch}) on the mobilisation of root-reinforcement was investigated.
2. Similar to Scenario 1, but with much thicker roots (d_{main} = 10 mm, d_{branch} = $d_{main}/3$) to provide a contrasting case for the thin roots observed in the CT scans. All other parameters were the same as in Scenario 1.

All root ends were modelled as free (no internal forces within the root in any degree of freedom). Therefore, given the assumed isotropic stress conditions only half of the root ($0 \leq X \leq 250$ mm was modelled because of symmetry.

3 Results

3.1 Scenario 1: Roots in the CT scanned direct shear tests

Decreasing the distance between branches significantly increased the root-reinforcement that could be mobilised (Figure 3a) and increases the mobilisation rate of the reinforcement. In contrast to the unbranched case, cases with small branching distances continued to mobilise more reinforcement even after direct shear displacements of 30 mm, suggesting their peak reinforcement capacity is higher.

The main axis of all modelled 1.5 mm diameter roots, branched or unbranched, was found to follow the deformation of the soil almost perfectly (Figure 3b). Decreasing the branching distance only slightly affected the position of the deformed main root axis. The increased root anchorage due to the presence of branches increased the axial stresses in the main root by a small amount (Figure 3c) while reducing the bending stresses (Figure 3d). The increase in root-reinforcement with increasing branching is almost entirely due to an increase in root internal normal force rather than internal shear force at the shear plane (Figure 4).

The maximum axial and bending stresses in the main root (L_{main}/s_{branch} = 17) at 20 mm shear displacement were 5.6 and 6.0 MPa respectively. In side branches, the maximum axial stresses were lower (1.4 MPa) but bending stresses higher (36.3 MPa).

3.2 Scenario 2: Large diameter roots

When thick roots (d_{main} = 10 mm) are modelled, absolute values of reinforcement are higher, although smaller fractions of the available strength are mobilised (Figure 5a). Compared to the thin d_{main} = 1.5 roots, the larger bending resistance causes these roots to 'dig' through the soil more, an effect increased by adding side branches ((Figure 5b).

Similar to scenario 1, adding more branches mostly increased tensile stresses and has only a small effect on

bending stresses (Figure 5c,d). This is reflected in the relative contributions of internal axial and shear forces in the root: a significant component of reinforcement in the unbranched case is caused by shear forces in the root, but this component hardly increases with an increased number of branches (Figure 4).

The maximum axial and bending stresses in the main root (L_{main}/s_{branch} = 17) at 20 mm shear displacement were 2.0 and 6.7 MPa respectively. In side branches, the maximum axial stresses were lower (0.2 MPa) but bending stresses higher (7.5 MPa).

4 Discussion

The results show that side branching had a significant effect on the mobilisation and magnitude of root-reinforcement in direct shear tests performed by Bull et al. [10]. This can be understood by the increase in root anchorage within the soil: to reach the same amount of shear displacement, more axial and transverse soil resistance has to be overcome in case the root is branched. This will have resulted in faster mobilisation of root-reinforcement and a suppression of root slippage. This shows that ignoring root branching in root-reinforcement calculations results in a conservative estimation of additional root strength.

The addition of branching results in larger relative transverse soil–root displacements: the displaced root tried to 'dig' through the soil in the transverse direction more. However, due to the relatively large transverse soil–root interface resistance (q_l) compared to the axial resistance (q_a), the deformed shape of the root is only minimally affected in the case of d_{main} = 1.5 mm roots. Thicker roots (d_{main} = 10 mm) underwent larger relative transverse soil–root displacement due to their larger bending resistance.

The analyses demonstrated the importance of a coupling between axial and bending behaviour of the root. In line with Equation 2, an increase in axial root stress (due to branching) resulted in partial suppression of root bending. The presence of branching however has a much larger effect on the internal axial forces in the root compared to the effect on the internal shear forces.

The high bending stresses in the side branches, compared to the axial stresses, indicates side branches were mostly loaded in bending rather than tension. This suggests that most of the additional root-reinforcement caused by branching was caused by mobilisation of transverse soil–root resistance along the side branches. This highlights the importance of understanding the behaviour of roots in bending. Little data is available on the bending strength and stiffness of roots as root strength is typically measured in uniaxial tension only. Future research should address this knowledge gap.

The analyses show that none of the main roots in direct shear tests by Bull et al. [10] is expected to have failed in tension when reaching the maximum shear displacement of 20 mm. Furthermore, roots are expected to follow the deformation profile of the soil almost perfectly. Both observations are confirmed by initial observations [10].
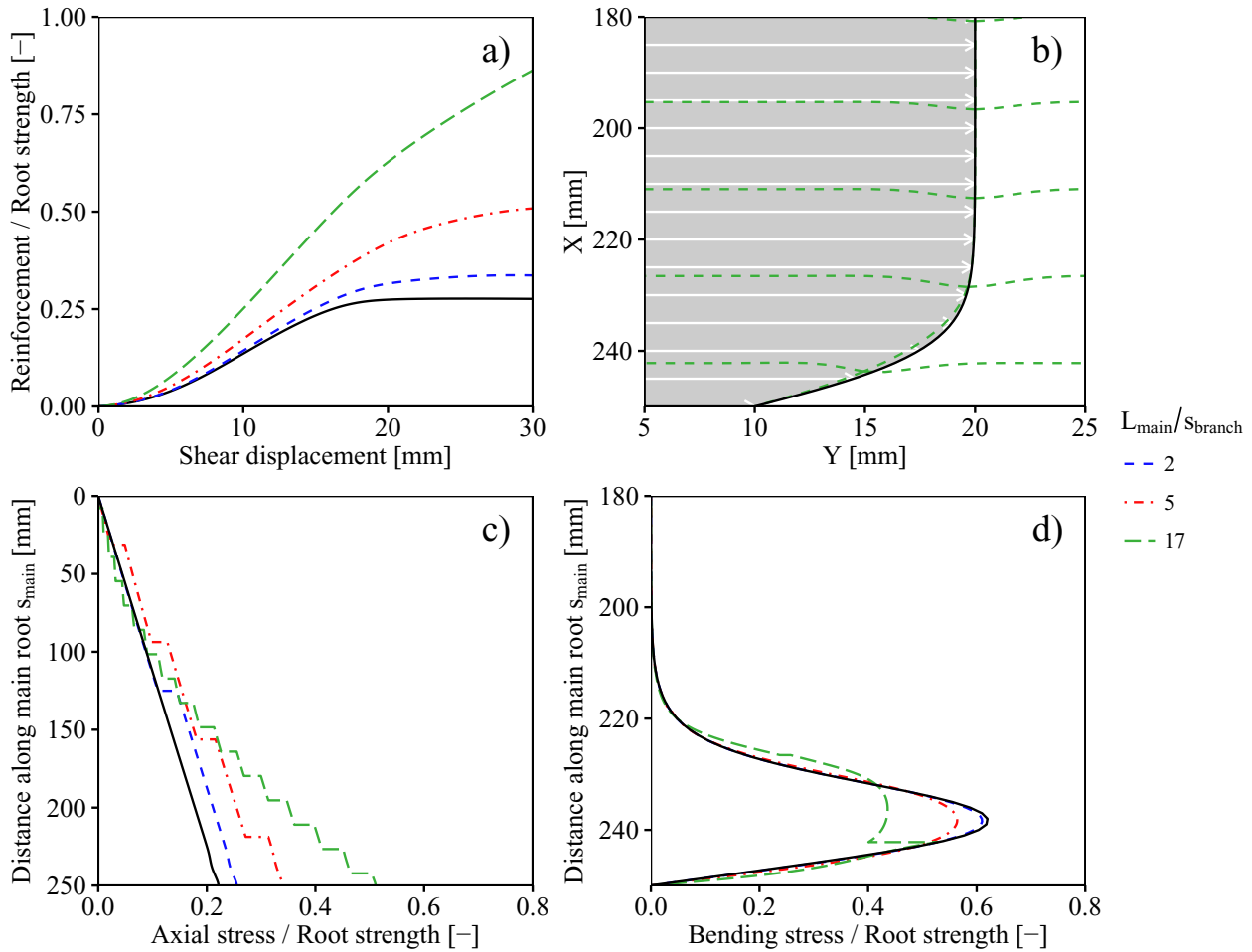
Fig. 3. Influence of branching distances for 1.5 mm diameter roots observed in the CT scan (Scenario 1). In (a,c,d), stresses are normalised against the root tensile strength. The unbranched case is plotted using solid, black lines. In b), the profile of soil deformation is indicated using the grey shaded area and white arrows. Axial (c) and bending stresses (d) are plotted for the main root axis only, where s_{main} indicated the distance along this axis (in the undeformed state) measured from the top of the root.
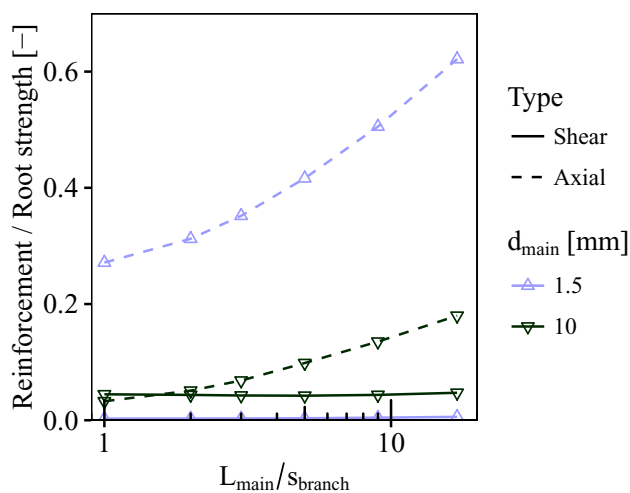

Fig. 4. Contributions of internal root normal and shear forces towards root-reinforcement as function of branching distance, at a shear displacement of 20 mm. Reinforcements are normalised by the maximum tensile strength of the root.

In this study a two-dimensional problem was investigated, assuming all roots were located on the same plane. Future work should focus on expanding the model into three-dimensions, so that more realistic root architectures can be analysed.

5 Conclusions

This study confirmed that the model, using large-deformation Euler-Bernoulli theory, is a relatively simple but powerful tool for studying the complicated effects of root architecture on the mobilisation and magnitude of root-reinforcement. The complex interaction between soil and root architecture can be captured using a set of coupled differential equations and relations describing the soil resistance to axial or transverse root displacements.

This study confirmed that side branching can have a significant effect on the rate of mobilisation and the maximum achievable mobilised root-reinforcement. The presence of branches counteracts potential slippage between soil and root, allowing for mobilisation of larger axial forces within the root and thus larger root-reinforcements.
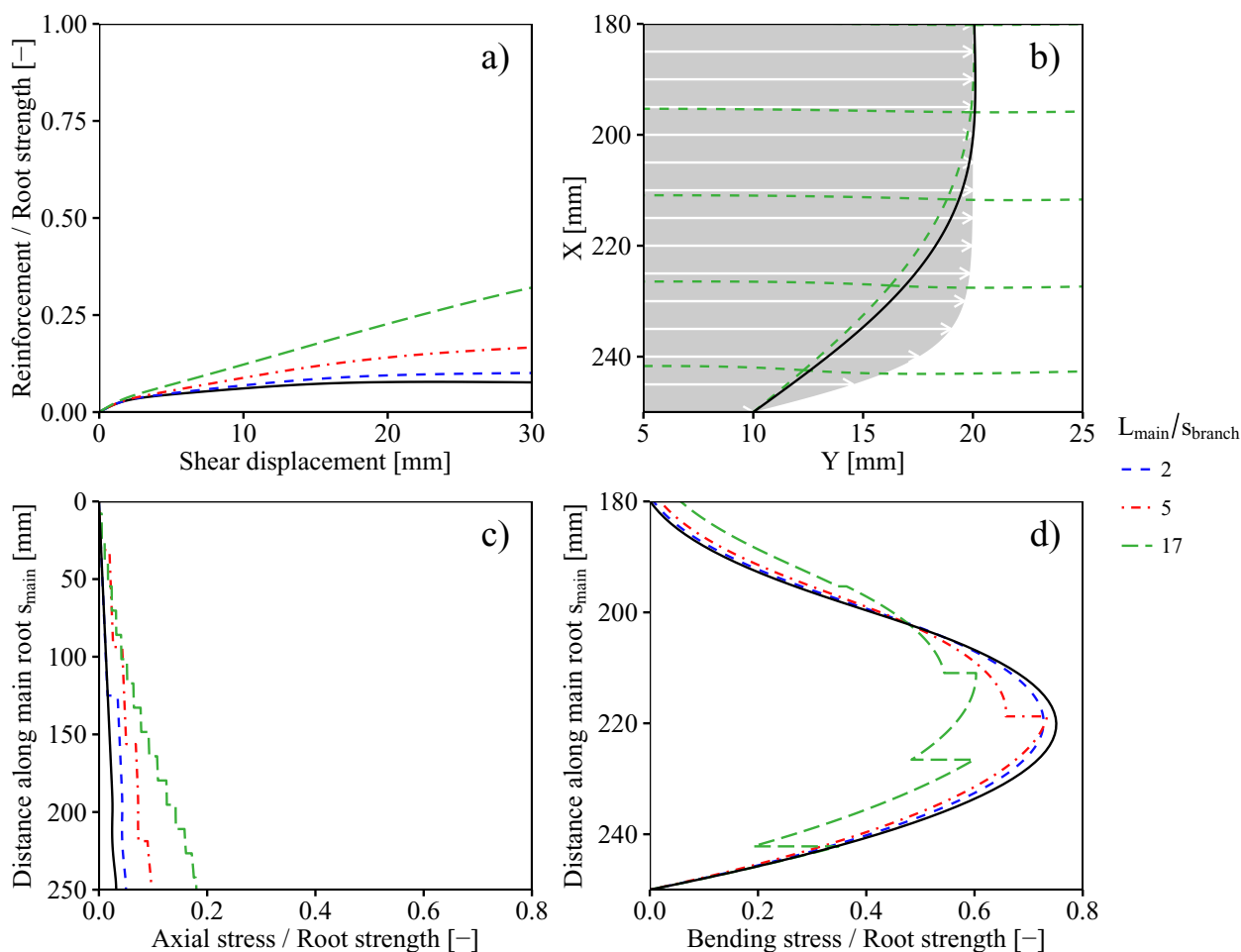
Fig. 5. Influence of branching distance for thick 10 mm diameter roots (Scenario 2). In (a,c,d), stresses are normalised against the root tensile strength. The unbranched case is plotted using solid, black lines. In b), the profile of soil deformation is indicated using the grey shaded area and white arrows. Axial (c) and bending stresses (d) are plotted for the main root axis only, where s_{main} indicated the distance along this axis (in the undeformed state) measured from the top of the root.

Observations by [10], including lack of root failure and roots following the pattern of soil deformation closely, were predicted correctly by the model.

References

[1] D.H. Gray, R.B. Sotir, *Biotechnical and soil bioengineering slope stabilization, a practical guide for erosion control* (John Wiley & Sons Inc, New York, 1996)

[2] L.J. Waldron, Soil Sci Soc Am J **41**, 843 (1977)

[3] N. Pollen, A. Simon, Water Resour Res **41**, W07025 (2005)

[4] T.H. Wu, R.M. McOmber, R.T. Erb, P.E. Beal, J Geotech Eng-ASCE **114**, 1351 (1988)

[5] T. Liang, J. Knappett, N. Duckett, Géotechnique **65**, 995 (2015)

[6] G.J. Meijer, D. Muir Wood, J.A. Knappett, A.G. Bengough, T. Liang, Int J Numer Anal Met (2018), advance online publication. DOI: 10.1037/a45d7867

[7] T. Liang, A.G. Bengough, J. Knappett, D. Muir Wood, K.W. Loades, P.D. Hallett, D. Boldrin, A.K. Leung, G.J. Meijer, Ecol Eng **109**, 207 (2017)

[8] G.J. Meijer, A.G. Bengough, J.A. Knappett, K.W. Loades, B.C. Nicoll, Géotechnique **68**, 320 (2017)

[9] E. Jones, T. Oliphant, P. Peterson et al., *SciPy: Open source scientific tools for Python* (2001–), http://www.scipy.org/

[10] D. Bull, I. Sinclair, F. Pierron, T. Roose, J. Smethurst, in *Proceedings of the 7th International Symposium on Deformation Characteristics of Geomaterials (IS-Glasgow 2019)* (2019)

[11] G.J. Meijer, A.G. Bengough, J.A. Knappett, K.W. Loades, B.C. Nicoll, Géotechnique **66**, 27 (2016)